DOI: https://doi.org/10.68732/9d243fcd44b1b733

ISBN: 978-9989-2053-6-1

Numerical investigation of fluid flow in intersecting fractures based on photogrammetry

M. Torkan, S. L. Vidanage, L. Uotinen, M. Janiszewski & M. Rinne
Department of Civil Engineering, School of Engineering, Aalto University, Espoo, Finland
masoud.torkan@aalto.fi
0000-0002-2102-0946

Abstract

Fluid flow through fractured rock networks is controlled by several factors, including hydraulic pressure gradients, fracture density, roughness, aperture, connectivity, and intersections. Characterizing hydraulic behaviour at fracture intersections is essential for understanding flow in rough fractured rock masses, especially for nuclear waste disposal.

In this study, a block of Finnish Kuru granite (10 cm × 10 cm × 10 cm) was prepared with two perpendicular and intersecting fractures. Photogrammetry was applied to reconstruct three-dimensional (3D) point clouds of the sample. To scale 3D models obtained by photogrammetry, markers with predefined distances were used, and accuracy was assessed by using Root Mean Squared Error (RMSE).Subsequently, roughness and physical aperture of fractures were quantified. The 3D point clouds were converted into a mesh domain in MeshInspector and imported into COMSOL Multiphysics, where fluid flow was simulated by solving the Navier–Stokes equations. Simulations were conducted under hydraulic pressure gradients ranging from 10 to 180 kPa/m, in increments of 10 kPa/m. The influence of intersections on flow for two inlets and two outlets was investigated. The Forchheimer equation was used to analyze the numerical results.

The photogrammetric reconstruction accuracy yielded an RMSE of 15 µm. Physical apertures for the two inlets were 190 and 192 µm, while for Outlets 1 and 2, they were 177 and 192 µm, respectively. 3D Roughness values were similar, ranging from 8.7 to 9.3. Numerical results showed nonlinear flow behavior at the outlets. The Forchheimer fitting was used to calculate hydraulic apertures and nonlinear parameters. A higher flow rate with a larger physical aperture, demonstrating the role of geometry in flow distribution.

This research shows that fracture intersections influence fluid flow behavior, leading to discharge changes based on geometrical properties, such as physical aperture. These factors must be considered in fracture network flow analysis.

Keywords

Intersecting fracture, Roughness, Photogrammetry, Numerical modelling, Fluid flow.

1 Introduction

The study of rock masses is essential because they serve as the foundation for critical infrastructure projects, including dams, tunnels, slopes, and nuclear waste disposal sites. A rock mass consists of intact rock and discontinuities, the latter of which govern both structural stability and fluid flow behaviour. In low-porosity rocks like granite, discontinuities, specifically faults and fractures, act as the primary pathways for fluid flow. Consequently, studying and characterizing discontinuities is vital for assessing the hydraulic properties of the rock mass. Fluid flow through fractures is controlled by several factors: at the micro-scale, by geometrical properties such as roughness, physical aperture, and contact area; and at the macro-scale, by fracture distribution, intensity, persistence, and density (Wyllie 1999).

The assessment of hydraulic properties has been conducted at various scales, from single fractures (Torkan et al. 2026) and intersecting fractures (Wang et al. 2025) to fracture networks (Baghbanan and Jing 2007). In single fractures, flow is primarily controlled by roughness and physical aperture, both of which are influenced by normal and shear stress distributions. Conversely, flow through intersecting fractures is further influenced by the angle of intersection (Xiong et al. 2020) and the number of inlets and outlets (Liu et al. 2025). Fluid flow in these systems is typically described by the Cubic Law or by nonlinear behaviour. The transition from the Cubic Law to nonlinear flow is rooted in the hydraulic gradient and in detailed geometrical properties (roughness, aperture, and contact points) of single fractures, as well as in intersection angles and fracture connectivity in intersecting systems.

Characterization of these features is achieved through various high-resolution methods, such as 3D laser scanning and photogrammetry. These methods allow for a realistic simulation of rock mass geometry. Laser scanning is a widely used tool for measuring roughness, physical aperture, and displacements, as well as for extracting fracture networks and simulating fluid flow. Similarly, photogrammetry has emerged as a low-cost, highly accurate alternative for measuring these same parameters. High-detail 3D models obtained via photogrammetry provide a cost-effective basis for simulating fluid flow. Previous studies have employed software such as ANSYS code (Xiong et al. 2020) and COMSOL (Liu et al. 2025; Wang et al. 2025) to investigate flow behaviour under various conditions of intersecting fractures with varying angles and inlet/outlet configurations.

Despite these advancements, the measurement of the actual geometrical properties of intersecting fractures and the use of that data as initial input for fluid flow simulations remains an area requiring further clarity. This study aims to demonstrate the use of photogrammetry to measure the geometrical properties of two nearly perpendicular intersecting fractures for use in COMSOL to simulate fluid flow. The Forchheimer equation was employed to characterize the numerical results regarding flow rates at two outlets versus hydraulic pressure gradients.

2 Methodology

2.1 Sample preparation

To investigate fluid flow behaviour in intersecting fractures, a Finnish Kuru grey granite block was first split from the centre using the feather-and-plug technique. The resulting separated block was cut into a 10 cm × 10 cm × 10 cm cube. Subsequently, a normal loading instrument was used to propagate an orthogonal fracture nearly perpendicular to the initial split (Fig. 1 (a)). This process resulted in a sample composed of four blocks (B1 to B4) separated by two nearly perpendicular fractures (Fig. 1 (c to f)).

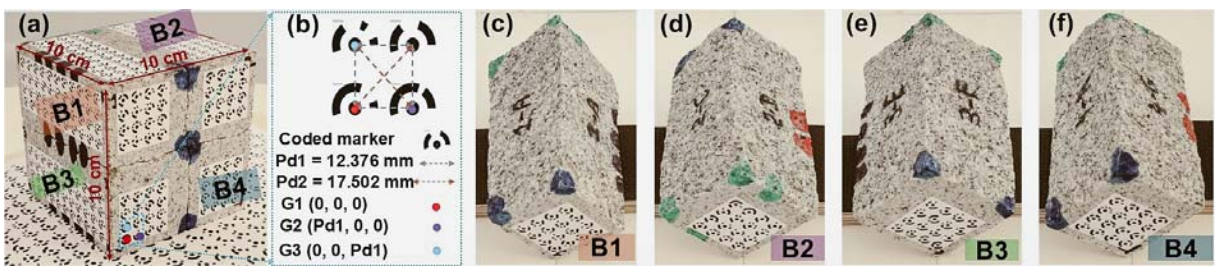


Fig. 1(a) The Kuru granite sample with dimensions of 10 cm × 10 cm × 10 cm, (b) markers with predefined distances and the defined local coordinate system; (c) Block B1; (d) Block B2; (e) Block B3; and (f) BlockB4.

2.2 Photogrammetry

2.2.1 Principle of photogrammetry

A Structure-from-Motion and Multi-View Stereo (SfM-MVS) photogrammetry approach was employed for 3D scanning. Photogrammetry is a technique that utilizes multiple overlapping photographs to reconstruct a 3D model by identifying and aligning matching points across images. This process generates a sparse 3D point cloud, which is then used to calculate depth maps to generate a high-resolution dense 3D point cloud. Specialized patterns, such as coded markers, are used to facilitate alignment and provide accurate scaling. By defining the distances and coordinates between these markers, the 3D model can be scaled and oriented within a specific coordinate system. In this research, RealityCapture software v1.5.1 was used for 3D modelling, utilizing self-calibration based on the Brown3 Tangential 2 distortion model. The final 3D models were exported as point clouds and analysed using CloudCompare software v2.14.

2.2.2 Sample preparation for photogrammetry

First, one-ring-20-bit-coded markers were generated via software, and the distances between them were measured digitally using AutoCAD. These markers were printed at 1200 dpi resolution and attached to the sample (Fig. 1 (a and b). Then the markers covering the fractures' outcrops were removed. The predefined horizontal and vertical distances between markers (Pd1) were 12.376 mm, while the diagonal distance (Pd2) was 17.502 mm.

2.2.3 Photography setup

The sample was placed at the centre of a rotary table (Fig. 2 (a)), with a sheet containing predefined alignment patterns (not used for scaling) placed beneath it. Illumination was maintained at a constant 4000 Lux. The rotary table was rotated in 9° increments over a full 360°, resulting in 40 photos per rotation. A Canon DSLR camera, equipped with a 35 mm lens, was mounted on a tripod at a fixed shooting distance of 50 cm. The camera specifications included a pixel size of 4.17 µm, a sensor size of 36 × 24 mm, and an image resolution of 8688 × 5792 pixels. The acquisition settings were an aperture of f/11 and a shutter speed of 1/8 s. This configuration yielded a Ground Sample Distance (GSD) of 59 µm, ensuring that each pixel represents 59 µm in the real world. The lens was manually focused on the fixed shooting distance, and the focus ring was secured with tape to prevent accidental shifts during photographing. The accuracy was further refined by the photogrammetry software, achieving sub-pixel precision ranging from one-fifth to one-twentieth of a pixel.

2.2.4 Photography workflow

To accurately measure the physical aperture of the intersecting fractures, the sample was photographed in a well-matched position (Fig. 2 (a)). To ensure sufficient image overlap and geometric coverage, photographs were taken at three different pitch angles: 0°, 30°, and 60°, using varying focus points. To increase the number of matching points across different images, an A4 sheet containing coded markers with predefined distances was placed beneath the sample. Each of the four blocks was then photographed separately using the two pitch angles, 30°and 60°, with two focus points per position to ensure depth of field and sharpness across the fracture surfaces (Fig. 2 (b)).Each block was subsequently flipped upside down, and the entire photography process was repeated (Fig. 2 (c)). For this stage, the marker sheet under the sample was not used.

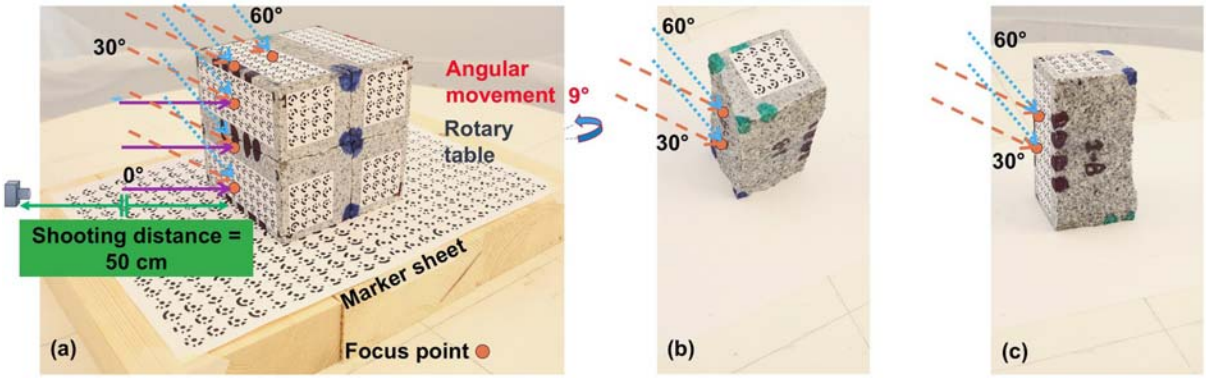


Fig. 2 Photography setup with a 50 cm fixed shooting distance and a rotary table with 9° angular movements. (a) The sample in the well-matched position showing the five different focus points photographed at pitch angles of 0°, 30°, and 60°. (b) and (c) illustrate the focus points on the blocks and the photography pitch angles before and after flipping the sample upside down. For example, (b) shows B1 photographed at 60°, and (c) shows B1 photographed upside down at 30°.

2.2.5 3D model reconstruction

The photograph set of the well-matched sample was imported into RealityCapture and grouped to ensure a consistent calibration across all images. After the software detected the markers, an initial alignment was performed. This well-matched 3D model served as a reference to establish the local coordinate system and to scale the model using the markets with the predefined distances (Fig. 1 (a)). To orient the model within a precise 3D space, the bottom corner of "Side One" was redefined from a tie point to a Ground Control Point (GCP) with coordinates G1 (0, 0, 0). Subsequently, the nearest horizontal and vertical markers were assigned GCP status with coordinates G2 (Pd1, 0, 0) and G3 (0, 0, Pd1), respectively. The 1133 predefined distances between these markers were used as scale bars (800) and check bars (333) to ensure dimensional accuracy. The model was then re-aligned to finalize the scaling and orientation within this desired coordinate system. Then, the coordinates of all detected markers on the sample were extracted. These coordinates acted as the references to put each block into the same coordinate system as the original well-matched sample. The same workflow was applied to each block. However, for these separate components, the 3D models were reconstructed with high detail and texturizing to measure physical aperture and roughness analysis.

2.2.6 Accuracy assessment

Root Mean Square Error (RMSE) (Eq. 1) was employed to assess the accuracy of the photogrammetry model. The obtained photogrammetric values for 800 scale bars and 333 check bars were compared with their real physical values after scaling.

$$RMSE = \sqrt{\sum_{i=1}^{n} \frac{(Predefined\ distance_i - digital\ distance_i)^2}{n}} \quad (1)$$

Here, i = the index of each predefined distance and n = the total number of predefined distances employed for scaling or checking.

2.3 Roughness and physical aperture

To measure roughness (R_{3D}), the two rough surfaces of each block were separated from the edge where the two rough surfaces reached each other. The 3D point cloud was rasterized at a resolution of 0.5 mm × 0.5 mm in the X and Y directions, converted to a mesh, and analyzed by the Surface Roughness Calculator (SRC) (Magsipoc et al. 2020). To measure physical apertures, the distances between two opposite surfaces were calculated in CloudCompare, and the averages of the distances were reported as physical apertures.

2.4 Numerical modelling and theoretical background

To simulate fluid flow through intersecting fractures with two inlets and two outlets, COMSOL Multiphysics v6.4 was employed to solve the Navier–Stokes equations. To create a domain for the simulation, the rough surfaces of the blocks were imported into MeshInspector software, converted into a 3D mesh domain, and subsequently imported into COMSOL. To analyze flow simulations, the surfaces were hypothetically segmented into four distinct pairs of opposing surfaces (Fig. 3 (a and b)). The boundary conditions are illustrated in Fig. 3 (b). The final model contained approximately 2 million elements, including boundary elements Fig. 3 (c).

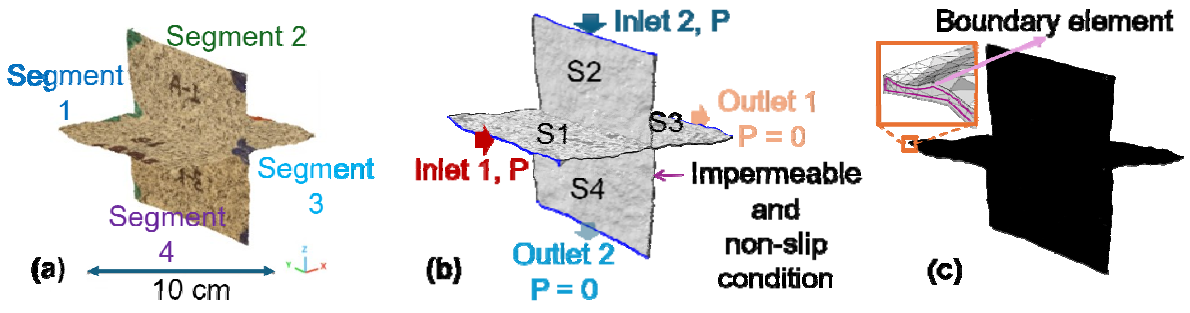


Fig. 3 (a) Segmentation of surfaces, (b) definition of boundary conditions in COMSOL, and (c) the final mesh model.

To analyze the relationship between the flow rate at the outlets and the hydraulic pressure gradients between the inlets and outlets, the Forchheimer equations (Eqs. 2-5) were used.

$$-\nabla P = AQ + BQ^2 \quad (2)$$

$$-\nabla P = \frac{\Delta P}{L} \tag{3}$$

$$A = \frac{12\mu}{we_h^3} \tag{4}$$

$$B = \frac{\beta\rho}{w^2 e_h^2} \tag{5}$$

Here, $-\nabla P$ (Pa/m) denotes the pressure drop (ΔP) over a length (L), and the terms AQ and BQ^2 represent linear and nonlinear flow rates, respectively. In this equation, Q (m^3/s) indicates flow rate, μ (8.9×10^{-4}Pa.s) signifies fluid viscosity, w (m) is fracture width perpendicular to flow, e_h is hydraulic aperture, β (m^{-1}) implies the non-Darcy coefficient related to fracture geometry, and ρ ($997kg/m^3$) is fluid density.

3 Results and discussion

3.1 Accuracy assessment, roughness, and physical aperture

The accuracy assessment of the 800 scale bars and 333 check bars yielded RMSEs of 14 μm and 15 μm, respectively. The aperture fields for each segment are illustrated in Fig. 4 (a to d). Additionally, the calculated R_{3D} and average physical apertures are reported within the same figures. Variations in R_{3D}were found to be negligible, ranging from 8.708 to 9.339. Notably, Segment 3 exhibited the highest roughness (9.339), while Segment 4 was the lowest (8.708). The physical apertures for the two inlets (Segments 1 and 2) were very similar, measuring 190 μm and 192 μm. However, the values for the outlets (Segments 3 and 4) showed a more significant difference of 18 μm, measuring 177 μm and 195 μm, respectively. It can be concluded that Segment 3 is rougher and tighter than Segment 4.

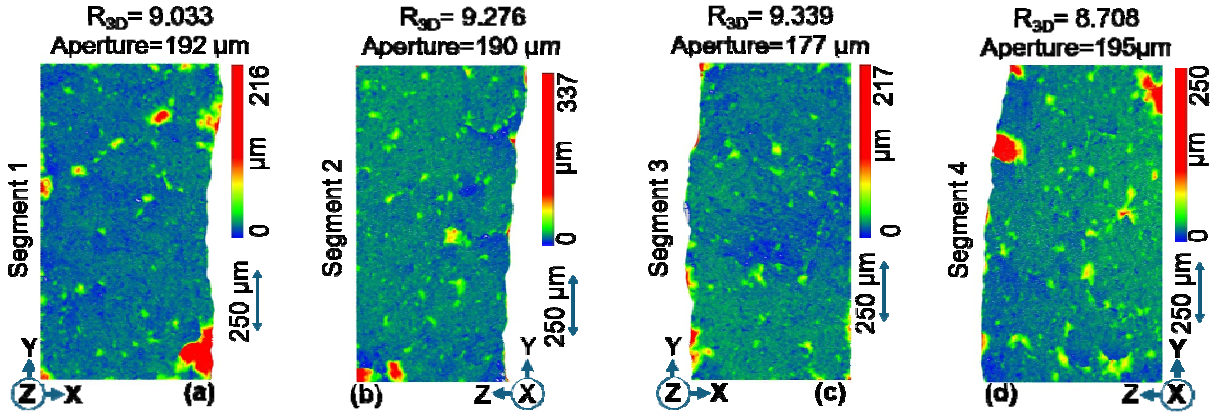


Fig. 4 (a) Physical aperture fields of (a) Segment 1, (b) Segment 2, (c) Segment 3, and (d) Segment 4. Roughness and physical apertures are provided for each segment.

3.2 Numerical modelling results

Fig. 5 (a) illustrates the Forchheimer equation fitted to the numerical results, showing the nonlinear relationship between the flow rate at the outlets and the hydraulic pressure gradient. The calculated hydraulic apertures (e_h) for Outlet 1 and Outlet 2 are 162μm and 175 μm, respectively. These results are consistent with the physical aperture measurements for these segments, where a higher physical aperture directly (Segment 4) corresponds to a higher hydraulic aperture.

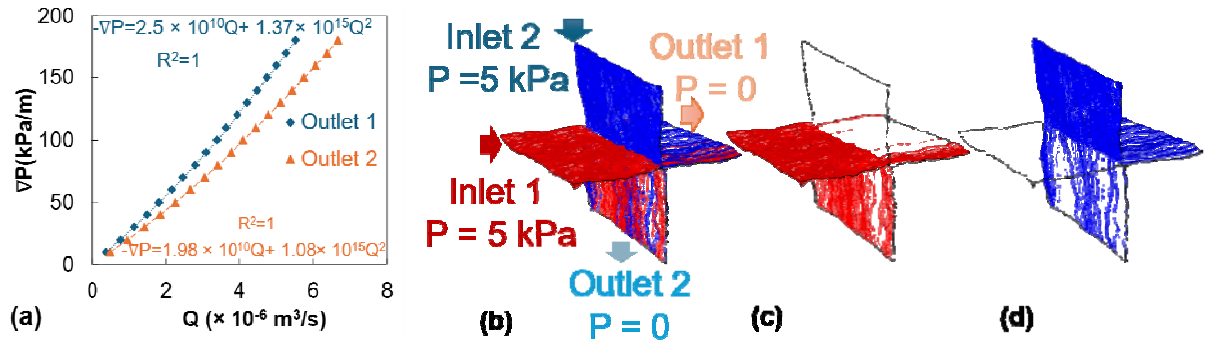


Fig. 5 (a) Nonlinear relationship between flow rate and hydraulic pressure gradient fitted by the Forchheimer equation; (b) streamline distributions of the two inlets at P = 5 kPa; (c) streamline distribution of Inlet 1; and (d) streamline distribution of Inlet 2.

The non-Darcy coefficients (β) were calculated as362 m^{-1} and 333 m^{-1}. This variation can be attributed to the differences in R_{3D}s and physical aperture sizes between Segments 3 and 4; specifically, Segment 3 is rougher and tighter than Segment 4. Fig. 5 (b) shows the streamline distribution originating from the two inlets. As observed, the streamlines from Inlet 1 primarily flow through Outlet 2 (Fig. 5(c)), while those from Inlet 2 exited through Outlet 1(Fig. 5(d)). Some mixing occurred within both Segments 3 and 4, which could be attributed to the intersection geometry and the configuration of the outlet segments. It seems mixing flow in Fig. 5(c) is lower than that in Fig. 5(d). This may be explained by the fact that Segment 4 (leading to Outlet 2) is wider and less rough than Segment 3 (leading to Outlet 1). Overall, it is evident that geometrical properties significantly influence the flow distribution. These intersecting fracture characteristics are critical for accurately analyzing fluid flow behavior within fracture networks.

4 Conclusion

In this study, photogrammetry was employed to reconstruct a 3D model of two intersecting fractures within a 10 cm × 10 cm × 10 cm domain. The accuracy assessment yielded an RMSE of 15 μm, demonstrating the capability of photogrammetry to reconstruct a highly accurate 3D model of a complex fracture intersection. This led to measuring physical apertures (177-195 μm) and surface roughness (R_{3D}, 8.708-9.339). Then, 36 fluid flow simulations were conducted using the 3D model in COMSOL across two inlets and two outlets using 18 different hydraulic pressure gradients (10 to 180 kPa/m).The results exhibited a nonlinear relationship between the hydraulic pressure gradients and the flow rates at the outlets. Fitting the Forchheimer equation to the numerical results showed that the tighter, rougher fracture segment resulted in lower e_h and higher β. Furthermore, the findings revealed mixing behaviour of fluid flow, indicating that fluid flow preferentially migrated toward the fracture segment with a higher physical aperture. These results emphasize that the intersection geometry and surface characteristics are critical factors in governing the flow distribution within fracture networks.

Acknowledgment

This work was funded by the Ministry of Economic Affairs and Employment of Finland as a part of the National Nuclear Safety and Waste Management Research programme (SAFER) in the research projects MIRKA I (funding number SAFER 23/2025) and MIRKA II (funding number SAFER 32/2026). During the preparation of this work, the authors used Gemini to check the language and improve readability. After using Gemini, the authors reviewed and edited the content as needed and take full responsibility for the content of the publication.

References

Baghbanan A, Jing L (2007) Hydraulic properties of fractured rock masses with correlated fracture length and aperture. International Journal of Rock Mechanics and Mining Sciences, 44(5): 704-719. https://doi.org/10.1016/j.ijrmms.2006.11.001

Liu J, Li C, Hu J, Luo Y, Liu B, Wang Z, Xie H (2025) Effect of stress-induced void heterogeneity and intersection geometry on heat transfer through 3D intersected rock fractures. Computers and Geotechnics, 186: 107429. https://doi.org/10.1016/j.compgeo.2025.107429

Magsipoc E, Zhao Q, Grasselli G (2020) 2D and 3D roughness characterization. Rock Mechanics and Rock Engineering, 53: 1495-1519. https://doi.org/10.1007/s00603-019-01977-4

Torkan M, Vidanage SL, Uotinen L, Janiszewski M, Rinne M (2026) Study on physical aperture and fluid flow behavior after dislocation of a rough fracture. International Journal of Rock Mechanics and Mining Sciences, 202: 106511. https://doi.org/10.1016/j.ijrmms.2026.106511

Wang XY, Zhong Z, Xie X, Hu Y, Han C, Lu B (2025) A nonlinear flow model and criterion for 3D natural fracture intersections: Effects of surface roughness and mechanical aperture. International Journal of Rock Mechanics and Mining Sciences, 193: 106169. https://doi.org/10.1016/j.ijrmms.2025.106169

Wyllie DC (1999) Foundations on Rock: Engineering Practice. London, CRC Press. https://doi.org/10.1201/9781482295009.

Xiong F, Wei W, Xu C, Jiang Q (2020) Experimental and numerical investigation on nonlinear flow behaviour through three dimensional fracture intersections and fracture networks. Computers and Geotechnics, 121: 103446. https://doi.org/10.1016/j.compgeo.2020.103446